Relaxation Dynamics of Entangled and Unentangled Multiarm Polymer Solutions: Experiment

Juliani and Lynden A. Archer*

School of Chemical Engineering, Cornell University, Ithaca, New York 14853-5201

Received March 29, 2002

ABSTRACT: Relaxation dynamics of several model $A_3-\mathbf{A}-A_3$ multiarm 1,4-polybutadiene melts and solutions are investigated experimentally using small amplitude oscillatory shear rheometry over a broad temperature range (−90 to +26 °C). Two rubbery plateaus are identified from loss $G''(\omega)$ minima at low frequencies. The storage modulus in the first plateau regime is of similar magnitude to the plateau modulus G_{N0} of entangled linear 1,4-polybutadiene melts, and varies with multiarm solution concentration ϕ_{pom} as $G_N(\phi_{pom}) = G_{N0}\phi_{pom}^{2.2\pm0.1}$. The second low-frequency plateau modulus $G_{N,II}$ increases with crossbar A volume fraction ϕ_{cb} in nearly the manner expected for dynamics of crossbar segments in a network diluted by relaxed arms, *A* (i.e., $G_{N,II} \approx G_N(\gamma_{pom})\phi_{cb}^{1+\beta}$, with $\beta \approx 1.3$). Despite this, we find that arms exert a profound influence on crossbar dynamics well after they have relaxed. Specifically, at solution concentrations below the threshold for arm entanglement, the zero-shear viscosity of multiarm solutions vary with ϕ_{pom} as $\eta_0 \sim \phi_{pom}^{2.9\pm0.2}$, which is slightly weaker than expected for entangled linear polymers without contour length fluctuations. However, for these same materials the terminal time λ is found to depend more strongly than expected on solution concentration, $\lambda \sim \phi_{pom}^{2.6\pm0.3}$. At polymer concentrations above the threshold for arm entanglements, a transition to much stronger terminal property scalings with solution concentration and molecular weight are observed. In particular, for arm entanglement densities above two, the zero-shear viscosity and terminal time of multiarm solutions are exponential functions of overall polymer molecular weight and concentration.

Introduction

Rheological studies of entangled branched polymers, particularly model long-chain branched (LCB) materials with well-defined architectures and molecular weights, have long been recognized as important for fundamentally understanding structure-processing relationships in commercial long-chain branched polyolefins. Results from such studies can also be used to evaluate predictions of branched polymer dynamics from recent molecular theories[1−3] and computer simulations.[4] The number of experimental studies of model LCB polymer dynamics has been limited, however, by a variety of factors, including the delicate chemistry involved in synthesizing model LCB structures and the difficulty of separating desired target structures from reaction byproducts.[2,3,5−9] It is nonetheless quite clear from published data that dramatic changes in dynamics occur when long entangled arms are appended to entangled linear molecules or, equivalently, when an entangled linear connector molecule bridges entangled starlike structures.[5−9]

Roovers, for example, reported zero-shear viscosity η_0 and recoverable compliance J_e^0 data for several narrow molecular weight distribution H-shaped ($A_2-\mathbf{A}-A_2$) polystyrenes dissolved in *n*-butyl benzene ($\phi = 0.255$ g/mL).[5] Polymers used in the study were synthesized with equal arm (*A*) and crossbar (**A**) molecular weights, in the range 1.93×10^4 to 2.04×10^5. For the lower molecular weight materials, Roovers found the same scaling dependence of zero-shear viscosity η_0 on polymer molecular weight as observed for linear polymers with comparable molecular weights. However, zero-shear viscosities for higher molecular weight, entangled H-shaped polymer solutions were significantly enhanced relative to η_0 values for linear polymers and starlike polymers of comparable molecular weight, suggesting that the connecting entangled arm (crossbar) in the H-shaped materials enhances overall flow resistance. In a related study, Roovers and Toporowski compared terminal relaxation times of hybrid star-comb polybutadienes possessing fixed crossbar molecular weight, but variable arm molecular weight, with terminal times of H-shaped polystyrene and starlike polymers (polybutadiene and polystyrene), also with variable arm molecular weight.[6] The authors found similar effects of arm molecular weight on relaxation time for all three architectures, underscoring the importance of arm molecular weight on viscoelastic properties of LCB polymers.

More recently, McLeish et al. studied linear viscoelastic behavior of H-shaped polyisoprene melts[2] and concluded that the frequency-dependent storage and loss moduli can be quantitatively described using a hierarchical theory for branched polymer dynamics proposed earlier by McLeish[1] and refined in ref 2. Daniels et al. recently extended the earlier comparisons to 50% and 20% solutions of H-shaped polyisoprene in squalene and found fair agreement between the theory and experiment.[7] Islam et al. performed the first systematic study of linear viscoelasticity in narrow distribution six-arm ($A_3-\mathbf{A}-A_3$) and eight-arm ($A_3-\mathbf{A}(A_2)-A_3$) 1,4-polybutadienes. In many of these materials, the arm molecular weight was held fixed, while the crossbar molecular weight was systematically varied.[9] The authors found that the frequency-dependent storage and loss moduli of the six-arm materials were fairly described by the theory of McLeish et al.,[2] but that terminal properties were much stronger functions of M_{cb} than expected from the theory. Islam et al., for example, reported that the terminal relaxation time and zero-shear viscosities of $A_3-\mathbf{A}-A_3$ polymers varied with crossbar molecular weight as, $\lambda \sim M_{cb}$;[7] $\eta_0 \sim M_{cb}$,[8] compared to the theoreti-

10.1021/ma0205010 CCC: $22.00
Published on Web 07/25/2002

Table 1. Molecular and Microstructural Characteristic of Multiarm Polybutadiene Melts

sample	M_w crossbar[a]	$\bar{M}_w$ arm[a]	M_w polymer[b]	M_w/M_n polymer	vinyl content[c] (%)
PB161			1.0×10^4	1.04	5.0
P1508_8 (8-arm)	4.2×10^4	2.02×10^4	21.5×10^4	1.13	4.8
P1184	3.87×10^4	1.46×10^4	12.8×10^4	1.15	21.8
P1589	8.9×10^4	2.1×10^4	21.03×10^4	1.04	18.6
P1207	9.62×10^4	2.01×10^4	21.5×10^4	1.12	19.3
P1625	15.1×10^4	2.2×10^4	26.7×10^4	1.06	15.1
MA1	10.4×10^4	1.9×10^4	17.6×10^4	1.12	8.5
MAll	7.7×10^4	1.8×10^4	22.5×10^4	1.25	8.8
MA12	7.7×10^4	4.4×10^4	39.9×10^4	1.28	9.2
MA15	10.1×10^4	3.7×10^4	32.2×10^4	1.19	11.4

[a] $\bar{M}_w$ of unlinked crossbar and M_w arms, from SEC. [b] Absolute $\bar{M}_w$ of multiarm polymer from SEC−multiangle laser light scattering analysis. [c] Vinyl content determined from H NMR measurements in deuterated benzene.

cal result, $\lambda \sim (M_{cb}/M_e)^2$, assuming hierarchical dynamics. Here M_e is the entanglement molecular weight.

Islam et al. also reported that the mean segmental relaxation time of the studied materials manifested a small, but systematic increase with increasing M_{cb}. The authors speculated that either a reduction in monomeric friction coefficient due to greater number of chain ends in the lower M_{cb} materials, or a systematic variation of vinyl (1,2-polybutadiene isomer) content with increasing M_{cb} could be responsible for the drift in segmental scale properties, and perhaps even for the stronger M_{cb} dependences of λ and η_0. However, even after transforming terminal properties to an isofrictional base (i.e., removing the inherent dependence of terminal properties on their segmental scale equivalents)[9] and renormalizing crossbar molecular weight to account for dilution by relaxed arms, Islam, et al. found that λ and η_0 remained stronger functions of crossbar molecular weight than expected from theory. The source of this behavior is to date unresolved.

The objective of the present study is two-fold: first, to examine the fundamental origin of the drift in monomer-scale frictional properties reported by Islam et al., and second, to determine the effect of systematic changes in arm and crossbar entanglement densities on terminal properties of model long-chain branched polymer liquids. The first objective is achieved using H NMR measurements and high-frequency (low temperature) compliance-free rheometry to characterize microstructure and monomeric scale properties of $A_3-\mathbf{A}-A_3$ multiarm LCB 1,4-polybutadienes. The second objective is satisfied using oscillatory shear rheometry of multiarmi/oligomer 1,4-polybutadiene blends covering a broad range of arm and crossbar entanglement densities.

Experimental Section

A. Materials. Various narrow molecular weight distribution (MWD) six-arm $A_3-\mathbf{A}-A_3$ 1,4-polybutadienes were synthesized using anionic living polymerization by Dr. S. K. Varshney (P-series materials, Table 1) of Polymer Source (Quebec, Canada) and by Professor Jimmy Mays' group (MA-series materials) at the University of Alabama, Birmingham, AL. Details of the synthesis scheme and fractionation procedures have been described previously.[8,9] Molecular weight averages and polydispersity indices of the unlinked arms and crossbars were determined using size-exclusion chromatography, with linear 1,4-polybutadiene standards as references. A SEC equipped with an on-line multiangle light-scattering characterization system was used to deduce similar information for the linked multiarm polymers. Table 1 summarizes information obtained from these measurements for all polymer samples used in the study.

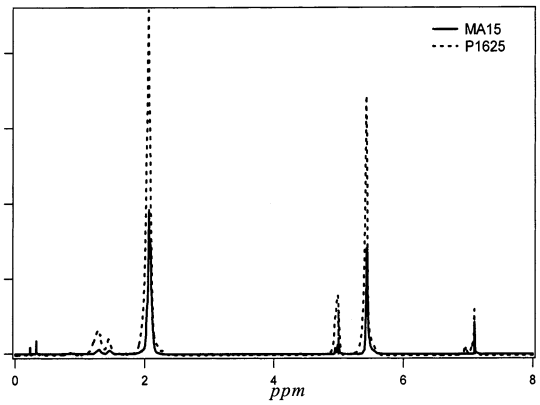

Figure 1. H NMR profiles for multiarm polymer samples P1625 and MA15 in deuterated benzene.

H NMR analysis of representative unlinked arms and crossbars indicated > 92% and approximately 55% 1,4-isomer content, respectively.[8] High-frequency oscillatory shear data reported by Islam et al. show that the mean segmental relaxation time τ_m of a linear polybutadiene with approximately 88% 1,2-isomer content exceeds that of a polybutadiene with approximately 92% 1,4-isomer content by a factor of about 12.[9] Thus, the microstructural content of 1,4-polybutadienes is anticipated to be an important determinant of τ_m. To determine what role, if any, systematic variations in microstructure played in the M_{cb}-dependent changes in τ_m reported by Islam et al., the MA series materials were synthesized under conditions designed to reduce the 1,2-isomer content. In addition, H NMR analysis was performed on all multiarm polymers to quantify their overall 1,2-(vinyl) isomer content.

Figure 1 illustrates typical pulse H NMR profiles of some of these materials in deuterated benzene. The 1,4-polybutadiene microstructure is identified by resonance peaks at 2.1 and 5.4 ppm, while the resonances at ca. 1.8 and 5 ppm arise from material with the 1,2-polybutadiene microstructure.[10] Vinyl contents estimated by integrating both 1,4- and both 1,2-resonances are provided in Table 1 for all materials used in the study. Although the results do reveal generally higher vinyl contents for the P-series multiarm polymers, very little change with M_{cb} is apparent for materials synthesized under the same conditions.

In an earlier study Juliani and Archer reported that terminal properties of bidisperse blends of high molecular mass linear 1,4-polybutadienes $M_{wL} = 5.15 \times 10^5$ g/mol and low molecular mass linear polybutadienes with $M_{ws} < 23M_e$ are independent of the low molecular polymer molecular weight.[11] In the present study, we therefore use linear 1,4-polybutadienes with $M_w = 1.1 \times 10^3$ g/mol as a solvent/diluent for the multiarm polymers. Such dilution is advantageous because it increases the frequency range over which terminal behavior is observed, and reduces the need for measurements at elevated temperature. The chemical similarity of polymer and diluent also removes any uncertainties about solvent effects on monomeric properties.

Solutions of the low molecular weight 1,4-polybutadiene and multiarm polybutadienes were formulated by dissolving desired amounts of the two polymers in dichloromethane (Aldrich, methylene chloride). Following complete dissolution, the cosolvent was driven off at room temperature over a period of about 3 days. A simple gravimetric procedure was used to verify that this time period was sufficient to remove all the cosolvent. Solutions containing various concentrations ϕ_{pom} of the multiarm polymers were formulated using this procedure. ϕ_{pom} was systematically varied in these materials to provide multiarm polymer liquids with arm and crossbar entanglement densities ranging from below unity (unentangled) to well above unity (well entangled).

Table 2. Rheological Parameters for the Multiarm Melts

sample	ϕ_{cb}[a]	η_0 (Pa·s)	λ (s)	τ_e (s)	$G_N \times 10^{-6}$ (Pa)	$G_{N,II} \times 10^{-5}$ (Pa)
P161		1.57×10^5	0.16	3.0×10^{-7}	1.01	
P1184	0.31	1.1×10^6	47.6	2.88×10^{-6}	1.28	1.1
P1589	0.41	6.50×10^7	1333.3	1.74×10^{-6}	1.19	1.66
P1207	0.44	9.80×10^7	1721.2	2.0×10^{-6}	1.22	1.89
P1625	0.47			1.26×10^{-6}	1.28	1.55
MAI	0.38	5.92×10^8	2053.4	2.92×10^{-7}	1.53	2.27
MAll	0.42	2.92×10^8	1250	2.75×10^{-7}	1.69	1.67
MA12	0.23			9.86×10^{-7}	1.50	
MA15	0.31			6.30×10^{-7}	1.49	

[a] $\phi_{cb} = M_{cb}/qM_a + M_{cb}$.

B. Linear Rheology Experiments. Linear viscoelastic properties of the multiarm materials formulated in part A were characterized by small-amplitude oscillatory shear measurements. Measurements were performed over a temperature range −90 to +26 °C using a Paar Physica Modular Compact rheometer (MCR300) equipped with 25 and 6 mm diameter stainless steel parallel plate fixtures and with a CTD600 temperature controller. Low-temperature regulation was achieved using liquid nitrogen. The smaller diameter plates were used for low-temperature measurements to reduce rheometer compliance errors in the glassy zone. In fact it was observed that, even for these small plate diameters, gaps in the range 0.6−1 mm were needed to completely reproduce glassy moduli for 1,4-polybutadiene obtained from dynamic mechanical analysis using torsional shear fixtures. To ensure linearity, strain amplitudes were varied from as low as 0.05% at low temperatures and high frequency (i.e., near the glassy or softening zone) to as high as 5% at room temperatures and low frequency (in the terminal zone). Oscillatory shear experiments at all temperatures and frequencies were also repeated at progressively lower strain amplitudes until material functions (e.g., $G'(\omega)$ and $G''(\omega)$) manifested no change in response to changes in shear strain.

Rheological information obtained from these experiments are summarized in Table 2 for undiluted multiarm 1,4-polybutadiene melts and in Tables 3−8 for several of the multiarm solutions studied. The average entanglement jump time $\tau_e \approx \omega_e^{-1}$ for these materials was estimated from the frequency ω_e at which the plateau and high-frequency Rouse dynamic regimes intersect.[12] The plateau modulus G_N was defined as the storage modulus $G'(\omega)$ value at the frequency (ω_{min}), where the loss modulus $G''(\omega)$ displays a local minimum (i.e., just before the $G''(\omega)$ upturn to the high-frequency Rouse

Table 3. Structural and Rheological Parameters for Multiarm P1184 Solutions

sample	ϕ_{P1184}	η_0 (Pa·s)	λ (s)	J_e^0 (Pa^{-1})	G_N (Pa)	$G_{N,II}$ (Pa)
P1184O10	0.11	2.2	6.8×10^{-4}	3.70×10^{-4}		
P1184O16	0.17	8.2	1.7×10^{-3}	4.50×10^{-4}	3.68×10^4	
P1184O22	0.22	51	2.1×10^{-2}	9.72×10^{-4}	4.69×10^4	
P1184O51	0.51	3333	0.4	1.64×10^{-4}	2.73×10^5	1.91×10^4
P1184O73	0.73	1.50×10^5	6.3	8.84×10^{-5}	8.89×10^5	6.03×10^4
P1184O86	0.86	3.15×10^5	20.0	3.84×10^{-5}	1.08×10^6	6.44×10^4

Table 4. Structural and Rheological Parameters for Multiarm P1589 Solutions

sample	ϕ_{P1589}	η_0 (Pa·s)	λ (s)	J_e^0 (Pa^{-1})	G_N (Pa)	$G_{N,II}$ (Pa)
P1589O05	0.05	0.95	8.7×10^{-4}	8.90×10^{-4}		
P1589O10	0.11	7.13	5.3×10^{-3}	9.50×10^{-4}	8.03×10^3	
P1589O17	0.17	21.0	1.0×10^{-2}	4.00×10^{-4}	2.77×10^4	
P1589O21	0.21	1.01×10^2	2.9×10^{-2}	2.85×10^4	4.73×10^4	6.66×10^3
P1589O31	0.32	2.15×10^3	0.2	1.70×10^{-4}	1.74×10^5	2.00×10^4
P1589O45	0.45	2.54×10^4	1.4	1.05×10^{-4}	3.27×10^5	3.68×10^4
P1589O66	0.66	5.90×10^5	.8	3.91×10^5	5.48×10^5	7.90×10^4
P1589O80	0.81	9.00×10^6	2.7×10^2	3.50×10^{-5}	1.10×10^6	1.12×10^5

Table 5. Structural and Rheological Parameters for Multiarm P1207 Solutions

sample	ϕ_{PI207}	η_0 (Pa·s)	λ (s)	J_e^0 (Pa^{-1})	G_N (Pa)	$G_{N,II}$ (Pa)
P1207O10	0.1	15.5	1.0×10^{-2}	9.10×10^3		
P1207O17	0.17	120.0	3.3×10^{-2}	5.80×10^{-3}	2.48×10^4	
P1207O40	0.39	5.48×10^4	2.9	8.42×10^{-5}	3.09×10^5	3.77×10^4
P1207O66	0.66	1.20×10^6	40.0	3.30×10^{-5}	4.76×10^5	7.59×10^4
P1207O70	0.69	5.40×10^6	1.1×10^2	2.69×10^{-5}	9.15×10^5	1.36×10^5

Table 6. Structural and Rheological Parameter of Multiarm P1625 Solutions

sample	ϕ_{P1207}	η_0 (Pa·s)	λ (s)	J_e^0 (Pa^{-1})	G_N (Pa)	$G_{N,II}$ (Pa)
P1625O10	0.1	35	3.3×10^{-2}	1.50×10^{-3}	7.54×10^3	
P1625O20	0.21	913	0.30	2.70×10^4	3.57×10^4	3.18×10^3
P1625O38	0.38	1.58×10^5	20.0	1.30×10^{-4}	1.85×10^5	2.12×10^4
P1625O59	0.59	3.13×10^6	3.2×10^2	6.34×10^{-5}	3.95×10^5	4.52×10^4
P1625O83	0.82	1.40×10^8	7.1×10^3	3.00×10^{-5}	7.21×10^5	8.50×10^4

Table 7. Structural and Rheological Parameters for Multiarm MA12 Solutions

sample	ϕ_{MA12}	η_0 (Pa·s)	λ (s)	J_e^0 (Pa^{-1})	G_N (Pa)	$G_{N,II}$ (Pa)
MA12O02	0.02	0.6	3.2×10^{-4}			
MA12O05	0.05	2.5	6.8×10^{-4}	9.56×10^{-4}	4.30×10^3	
MA12O10	0.11	43.2	7.0×10^{-3}	6.22×10^{-4}	1.89×10^4	
MA12O20	0.21	2.60×10^2	2.3×10^{-2}	2.50×10^{-4}	8.10×10^4	
MA12O30	0.30	1.83×10^3	0.8	$7.32 \times 10-4$	9.05×10^4	
MA12O33	0.33	1.78×10^4	28.6	1.00×10^3	1.58×10^5	
MA12O40	0.38	2.86×10^5	1.0×10^3	5.30×10^{-4}	3.09×10^5	3.82×10^3
MA12O50	0.51	6.80×10^6	1.0×10^4	2.58×10^{-4}	4.32×10^5	5.25×10^3
MA12O80	0.79	1.86×10^8	3.3×10^5	7.00×10^{-5}	1.26×10^6	1.20×10^4

Table 8. Structural and Rheological Parameter for Multiarm MA15 Solutions

sample	ϕ_{MA15}	η_0 (Pa·s)	λ (s)	J_e^0 (Pa^{-1})	G_N (Pa)	$G_{N,II}$ (Pa)
MA15O02	0.03	2.4	2.8×10^{-3}	2.59×10^{-4}		
MA15O04	0.04	7.8	8.8×10^{-3}	1.20×10^{-3}		
MA15O05	0.05	13.4	1.6×10^{-2}	1.60×10^{-3}		
MA15O06	0.07	30.3	3.0×10^{-2}	1.35×10^{-3}	4.10×10^{3}	
MA15O08	0.08	64.2	7.1×10^{-2}	$1.2\,0 \times 10^{-3}$	6.79×10^{3}	
MA15O10	0.1	2.31×10^{2}	0.2	1.05×10^{3}	1.48×10^{4}	
MA15O20	0.19	9.20×10^{3}	3.6	1.00×10^{35}	7.55×10^{4}	
MA15O30	0.31	8.55×10^{5}	6.3×10^{2}		1.43×10^{5}	6.40×10^{3}
MA15O40	0.39	5.50×10^{6}	3.7×10^{3}	-5	2.67×10^{5}	1.07×10^{4}

regime). For some polymers, a second minimum in $G''(\omega)$ was observed at low frequencies; the corresponding storage modulus $G_{N,II}$ values estimated using the same procedure are provided in Tables 2−8. As discussed previously by Islam et al.,[9] this second, low-frequency loss minimum is believed to arise from dilution of crossbar entanglements by relaxed arm segments.

Zero shear viscosities $\eta_0 = \lim_{\omega\to 0} G''(\omega)/\omega^2$ were determined from $G''(\omega)$ in the terminal region. Terminal relaxation times λ were estimated from plots of $\eta''(\omega)/\eta_0$ as the inverse of the frequency ω_M where $\eta''(\omega)/\eta_0$ manifest a local maximum in the terminal zone. This assignment was recently shown to be nearly exact $\omega_M^{-1} \approx \eta_0 J_e^0$ for linear 1,4-polybutadienes where the terminal response is well described by a single-mode Maxwell model.[13] In the present case, however, uncertainty in $J_e^0 = \lim_{\omega\to 0} G''(\omega)/\omega^2$ values for many of the materials prevented independent calculation of λ from η_0 and J_e^0 at the temperatures of our measurements. The assignment $\lambda \approx \omega_M^{-1}$ is also advantageous because it facilitates separate determination of λ and η_0, allowing the effect of multiarm polymer molecular weight on molecular drag and relaxation dynamics to be evaluated separately.

Results and Discussion

Master plots of storage $G'(\omega)$ and loss $G''(\omega)$ moduli for representative multiarm polymer melts and solutions are presented in Figure 2a−c. With few exceptions, these plots were constructed from data at discrete temperatures in the range −90 to +26 °C using time−temperature superposition with respect to a reference temperature of 26 °C. Both horizontal (a_T) and vertical (b_T) shift factors were employed in the construction. Vertical shift factors were used to correct for the density dependence on temperature, particularly near the glass transition temperature. Composite curves obtained in this manner cover nearly fourteen decades of frequency and report dynamics from segmental (glassy librations) to translational diffusion of entire molecules.

At the end of the high-frequency glassy zone, $G''(\omega)$ manifests a local maximum. The frequency ω_{max} at which this loss maximum occurs can be used to estimate the segmental hopping time $\tau_m \approx \omega_{max}^{-1}$ of the studied material.[9] Thus, for a pure MA15 melt $\tau_m \approx 0.4$ ns, which is nearly identical to the τ_m value of 0.42 ns for the MA12 melt. Both results compare reasonably well with τ_m values of the P-series materials. For example for pure P1625 τ_m was found to be 0.28 ns, for P1589, $\tau_m \approx 0.28$ ns, while for P1207 $\tau_m \approx 0.26$ ns . τ_m values for both multiarm series polymers are also close to the value $\tau_m \approx 0.2$ ns determined using PB161, an entangled linear 1,4-polybutadiene melt with approximately 5% 1,2-addition. These results clearly do not support a systematic increase in τ_m with increasing vinyl content or crossbar volume fraction. In fact, the changes in τ_m observed between the MA-series and P-series materials are well within the uncertainty of the procedure used to determine τ_m. τ_m values measured for the multiarm solutions were, however, observed to be consistently lower than those of the melts by about 1 order of magnitude. This observation can easily be traced to the much faster monomer scale dynamics of the low-molecular-weight polybutadiene used as solvent.

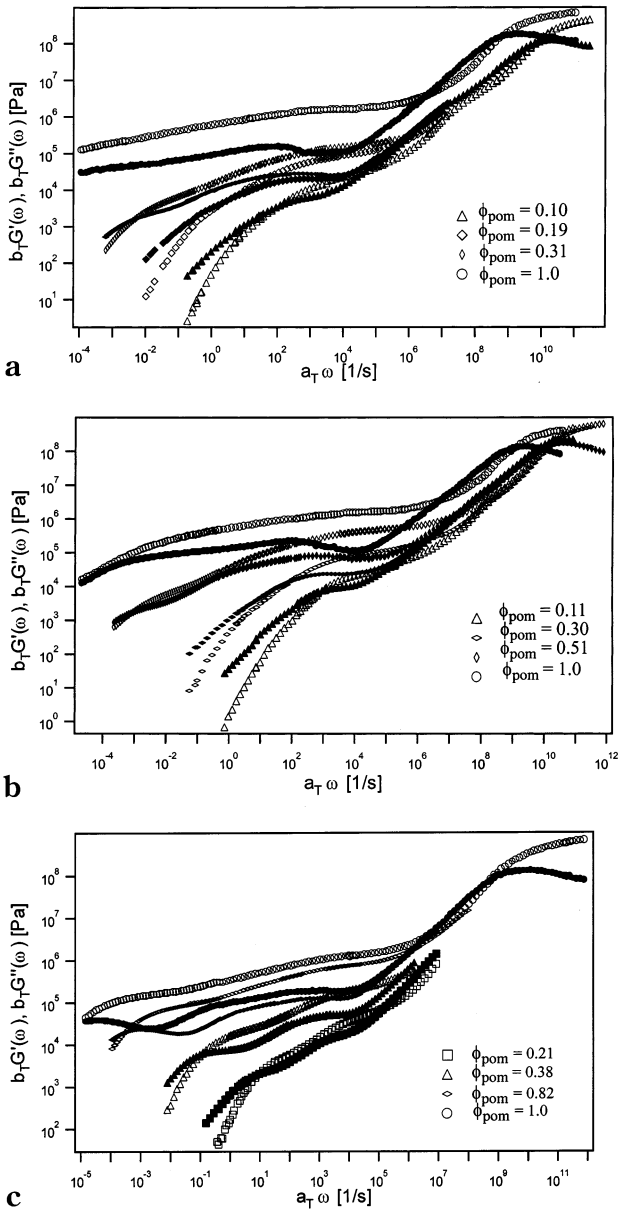

Figure 2. (a) Dynamic storage, $G'(\omega)$, and loss, $G''(\omega)$, moduli of MAS15 melt and solutions. Open symbols are $G'(\omega)$. (b) Dynamic storage, $G'(\omega)$, and loss, $G''(\omega)$, moduli of MA12 melt and solutions. Filled symbols are $G''(\omega)$. (c) Dynamic storage, $G'(\omega)$, and loss, $G''(\omega)$, moduli of P1625 melt and solutions. Open symbols are $G'(\omega)$.

Average entanglement Rouse times τ_e of multiarm melts are reported in Table 2. τ_e values for the two MA-series polymers are two to three times larger than those

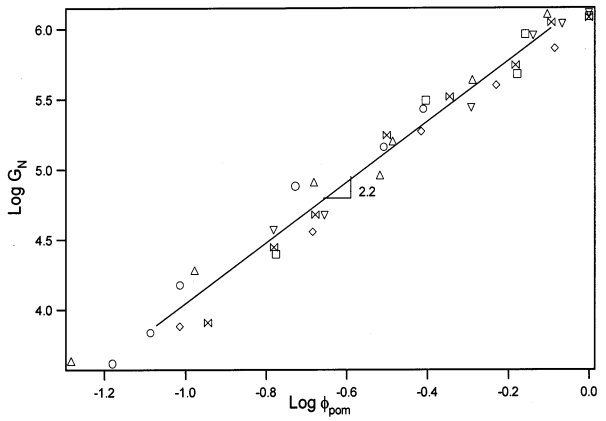

Figure 3. Effect of multiarm solution concentration on the rubbery plateau modulus, G_N.

of the linear 1,4-polybutadiene reference material, P161, while τ_e values for the P-series polymers are generally about a factor of about 7−9 times higher. P-series materials also show a gradual increase in τ_e with increasing vinyl content. The greater apparent sensitivity of τ_e (cf. τ_m) to vinyl content is not fully understood, but may be due to the additional effect of microstructure on entanglement molecular weight, $\tau_e \approx \tau_m N_e^2$ where $N_e = M_e/m_o$.

As the concentration ϕ_{pom} of multiarm polymer in solution is decreased, systematic reductions in storage and loss moduli are also clearly evident from the data (Figure 2, parts a−c). These changes can be better understood by considering how the entanglement plateau modulus G_N and *dilution* plateau modulus $G_{N,II}$ change with concentration. Figure 3 summarizes the effect of multiarm polymer concentration ϕ_{pom} on G_N values for several materials. The results support a simple relationship $G_N \sim \phi_{pom}^{\alpha+1}$, where $\alpha = 1.2 \pm 0.1$, in nearly perfect accord with expectations from theory.[14]

By definition, $G_{N,II}$ is anticipated to be determined by G_N and crossbar concentration in solution $\phi_{cb}\phi_{pom} = \phi_{pom}M_{cb}/(qM_a + M_{cb})$, where q is the number of arms per molecule. If $G_{N,II}$ is indeed the plateau modulus of the crossbar entanglement network following relaxation of arms, a relationship of the form $G_{N,II}/G_N \sim \phi_{cb}^{\beta+1}$ is expected as a consequence of crossbar constraints released by the relaxed arms. The ratio $\log(G_{N,II}/G_N)/\log \phi_{cb}$ can be determined for all materials where the low-frequency loss minimum is observed using data provided in Tables 2−8. It is apparent from the results that $\beta \approx 1.3$ for most of the polymers studied, confirming this assignment of $G_{N,II}$. However, for several of the studied materials (MA12, MA15, and P1625) β values well in excess of those expected on the basis of the simple dilution assignment are observed. Since β is most sensitive to the relative amounts of crossbar and arms in the materials, it is possible that the high β values originate from random variations in molecular structure (i.e., crossbar molecular weight M_{cb} and/or number of arms per crossbar, q; on the basis of the synthesis scheme, we do not anticipate variations in M_a). A comparison of the total multiarm weight-averaged molecular weight ($\bar{M}_{w,T} = \bar{M}_{w,cb} + 6\bar{M}_{w,a}$) with the overall weight-averaged multiarm polymer molecular weight from light scattering $\bar{M}_{w,LS}$ (Table 1) does indeed reveal differences in two of the three polymers (MA12 and P1625). Though the Δ values correspond roughly to the arm molecular weight($\Delta = \bar{M}_{w,T} - \bar{M}_{w,LS} = 1.6 \times 10^4$ for P1625, and $\Delta = -5.8 \times 10^4$ for MA12), the differences are too small and unsystematic to explain the larger β values observed.

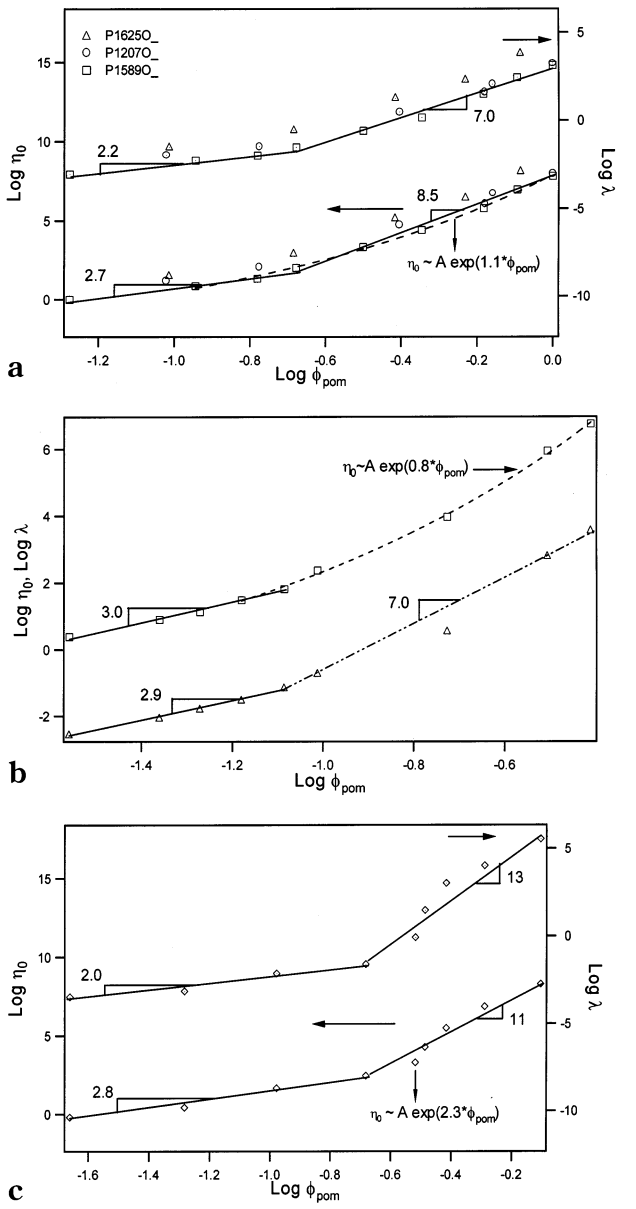

Figure 4. (a) Relaxation time λ and zero shear viscosity η_0 of several P-series A_3−**A**−A_3 multiarm polymer solutions with $M_a \approx 20 \times 10^3$ vs polymer weight fraction in solution. (b) Relaxation time λ and zero shear viscosity η_0 of MA15 as a function of polymer weight fraction in solution. (c) Relaxation time λ and zero shear viscosity η_0 of MA12 as a function of polymer weight fraction in solution.

Additional insight into multiarm polymer dynamics can be obtained by studying how terminal properties (η_0 and λ) vary with polymer concentration, arm entanglement density, and crossbar entanglement density. Figure 4a, for example, summarizes the effect of ϕ_{pom} on η_0 and λ for various P-series six-arm polymers with comparable arm molecular weights ($M_a = 2.1 \times 10^4$). Similar results for the two MA-series materials (MA120_, $M_a = 4.4 \times 10^4$ and MA150_, $M_a = 3.7 \times 10^4$) are provided in Figure 4, parts b and c, respectively. At low multiarm polymer concentrations, the P-series results support the following approximate scaling relationship: $\eta_0 \sim \phi_{pom}^{2.7}$ and $\lambda \sim \phi_{pom}^{2.2}$. Slightly stronger concentration dependences ($\eta_0 \sim \phi_{pom}^{3.0}$ and $\lambda \sim \phi_{pom}^{2.9}$) are observed for the MA15 solutions.

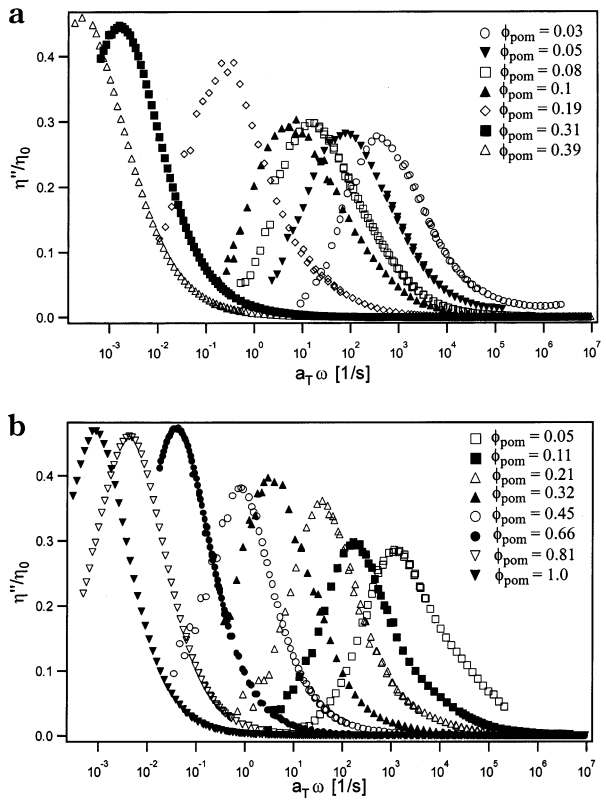

Figure 5. (a) Normalized imaginary component of complex viscosity $\eta''(\omega)/\eta_0$ for MA15 solutions at various concentrations. (b) Normalized imaginary component of complex viscosity $\eta''(\omega)/\eta_0$ for P1589 solutions at various concentrations.

Above a critical multiarm polymer concentration $\phi_{pom} = \phi_{pom}^* \approx 0.22$ for the P-series materials and $\phi_{pom}^* \approx 0.082$ for the MA150_ series polymers, both properties are seen to vary more strongly with concentration. The lines through the data support either a strong power-law dependence of λ and η_0 on concentration or an exponential concentration dependence. The transition in concentration dependence is also evident from plots of $\eta''(\omega)/\eta_0$ (see Figure 5, parts a and b). For $\phi_{pom} < \phi_{pom}^*$, the maximum value of $\eta''(\omega)/\eta_0$ is observed to be substantially below the result $\eta''(\omega)/\eta_0 = 0.44$ expected for a single Maxwell element, and observed for linear 1,4-polybutadiene melts.[13] This behavior is believed to reflect the greater range of relaxation modes in the dilute multiarm solutions. At multiarm concentrations above ϕ_{pom}^*, $\max(\eta''(\omega)/\eta_0)$ is observed to gradually increase as multiarm polymer concentration rises, eventually approaching values typical of linear 1,4-polybutadienes at high arm and crossbar entanglement densities.

The entanglement molecular weight of the multiarm polymer melts can be estimated from their plateau modulus using the relationship $M_{e0} = 0.8\rho N_A kT/G_{N0} \approx 1380$, where we have used $\rho = 0.9$ g/cm^3. This value for the melt M_e is somewhat lower than M_e values observed in pure 1,4-polybutadiene melts. The average entanglement molecular weight at ϕ_{pom}^* (i.e., $M_e^* \approx M_{e0}(\phi_{pom}^*)^{-1.3}$) is therefore approximately 9.88×10^3 for the P-series polymers, 1.05×10^4 for MA12, and 3.3×10^4 for the MA15O_ material. Thus, the observed transition occur close to the onset of arm entanglements. This statement is also supported by results obtained using P1184 (see Table 3), for which $\phi_{pom}^* \approx 0.27$, $M_e^* \approx 7.57 \times 10^3$, and $M_a/M_e^* \approx 2$.

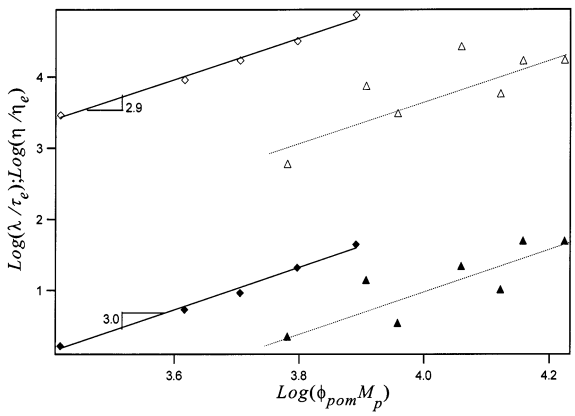

Figure 6. Relaxation times and zero shear viscosity vs renormalized crossbar entanglement density, $M_{cb}\phi_{pom}\phi_{cb}/M_{e0}$, for six-arm polymers with $(M_a\phi_{pom}/M_{e0}) < 2$. Triangles represent composite results for P-series polymers, and diamonds are results for MA15.

For $\phi_{pom} < \phi_{pom}^*$, the multiarm polymers might, therefore, be expected to manifest dynamics characteristic of moderately entangled linear polymers with centers of friction near the chain ends. Because of the larger arm friction near the chain ends, contour length fluctuations (CLF) are not expected to be as important as in the case of linear polymer molecules. In the absence of fluctuation effects, the zero-shear viscosity and terminal time of an entangled linear polymer in solution scale with polymer concentration ϕ as $\eta_0 \sim \phi^{1+2\alpha}$ and $\lambda \sim \phi^{\alpha}$, where $\alpha \approx 4/3$. When CLF are important these relations become $\eta_0 \sim \phi^{1+2.5\alpha}$ and $\lambda \sim \phi^{1.5\alpha}$. For $\phi_{pom} < \phi_{pom}^*$, the effect of ϕ_{pom} on zero-shear viscosity of the multiarm solutions is evidently close to the expected result for entangled linear polymer solutions in the absence of CLF. However, the terminal time increase more strongly with multiarm polymer concentration than expected, indicating that the analogy to an entangled linear solution is imperfect, even in LCB polymers with unentangled arms.

To remove uncertainties created by variations in polymer microstructure, η_0 and λ are normalized by the melt entanglement viscosity $\eta_e = G_N\tau_e$ and entanglement jump time τ_e, respectively. The combined effect of overall polymer molecular weight M_p and solution concentration ϕ_{pom} on normalized terminal properties of multiarm solutions with $\phi_{pom} < \phi_{pom}^*$ are summarized in Figure 6. The results presented for the P-series materials is a composite of solution data from several polymers; this we believe is the source of the scatter in the data. For comparative purposes, the figure also presents data for MA15 solutions. The solid lines through the MA15 data are "best-fits" to the data. Because of larger scatter of the P-series data, dashed lines through η_0 and λ results for these material are deliberately chosen with the same slope as the respective best-fit lines for the MA15 solutions. Both sets of results clearly support relationships between terminal properties and overall solution molecular weight that are quite similar to expectations for the linear polymers with suppressed CLF.

Parts a−c of Figure 4 also demonstrate that at multiarm polymer concentrations above ϕ_{pom}, η_0 and λ both increase as approximately exponential functions of concentration. To determine the source of this strong increase we consider separately the effects of variable *diluted* crossbar entanglement density $M_{cb}/M_e =$

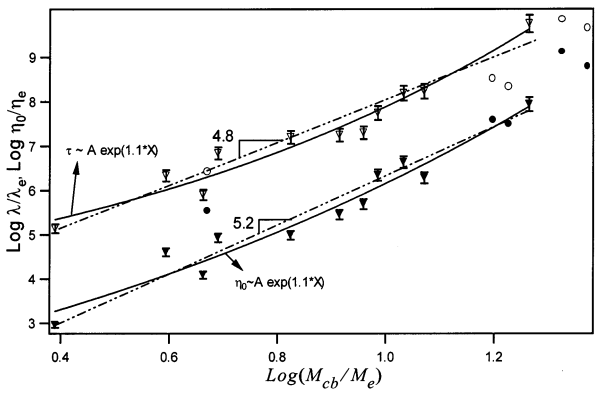

Figure 7. Plot of normalized terminal relaxation time λ/τ_e (open symbols) and zero shear viscosity η/η_e (closed symbols) vs crossbar entanglement density, $M_{cb}/M_e = M_{cb}(\phi_{pom}\phi_{cb})^{\alpha}/M_{e0}$. Triangles are composite results for solutions with M_a/M_e = 3−6 and circles are results for undiluted multiarm melts ($M_a/M_e \approx 10$).

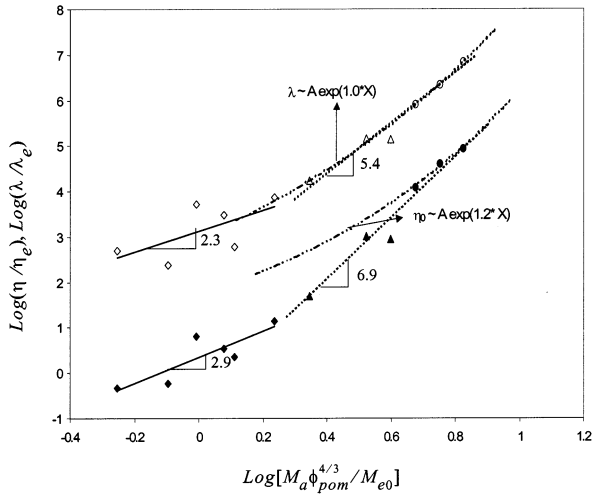

Figure 8. Plot of normalized terminal relaxation time λ/τ_e (open symbols) and zero shear viscosities η/η_e (closed symbols) vs arm entanglement densities, M_a/M_e, for A3−**A**−A3 1,4-po1ybutadienes with $M_{cb}/M_e < 1$ (diamonds), $M_{cb}/M_e \approx 2$ (triangles), and $M_{cb}/M_e \approx 4$ (circles).

$M_{cb}(\phi_{cb}\phi_{pom})^{4/3}/M_{e0}$ (at fixed arm entanglement density, $M_a/M_e = M_a\phi_{pom}{}^{4/3}/M_{e0}$) and of variable arm entanglement density (at fixed $\tilde{M}_{cb}/M_e = M_{cb}\phi_{pom}{}^{4/3}/M_{e0}$). Again the results presented are composites for several polymers. Figure 7, for example, presents results for multiarm polymers with two different range of arm entanglement density ($M_a/M_e \approx 3-6$, and $M_a/M_e \approx 10$). In both cases the terminal time and zero-shear viscosity are seen to vary rather strongly with crossbar entanglement density. The lines through the data in fact suggest that both properties are best described as exponential functions of M_{cb}/M_e. This finding is clearly important because it indicates that *even though a relaxed arm can dilute entanglements between crossbar segments* (e.g., as evidenced by the finding $G_{N,II}/G_N \sim \phi_{cb}{}^{1.3}$), *the presence of the arm nonetheless dramatically affects terminal crossbar dynamics*. Thus, the notion that the long-time dynamics of entangled multiarm polymers are similar to those of entangled linear molecules with higher friction is not supported by the experiments. It is nonetheless evident, from the form of M_{cb}/M_e, that fairly high initial crossbar entanglement densities are required to ensure that crossbars remain sufficiently well entangled in the terminal region for their dynamics to be constrained by tethering to the branch point.

Figure 8 shows the effect of arm entanglement density on terminal properties of six-arm polymers with fixed crossbar entanglement density M_{cb}/M_e. The data are again a compilation of results from several materials and is normalized by the respective entanglement viscosity η_e and entanglement Rouse time λ_e of the pure melt. It is apparent from the figure that, for $M_a/M_e > 2$, η_0 and λ are very strong functions of M_a/M_e. Taken together with the near exponential dependence of η_0 and λ on ϕ_{pom} for $\phi_{pom} > \phi_{pom}^*$ (see Figure 4a,b) and on M_{cb}/M_e, this result indicates that terminal properties of entangled the multiarm polymers are very likely exponential functions of the total polymer molecular weight. This finding is in fact consistent with the observation of Lusignan et al.[15] for commercial randomly branched polyester samples. Results from Figures 6−8 can be combined to yield the following empirical relations for terminal properties of multiarm polymers:

$$\eta_0 \approx \eta_e C_1\left[\left(\frac{M_{cb}}{M_e}\right)^3 + \left(\frac{M_a}{M_e}\right)^2 \exp\left\{\nu\left(\frac{M_a}{M_e} + \frac{M_{cb}}{M_e}\right)\right\}\right] \quad (1)$$

$$\lambda \approx \tau_e C_2\left[\left(\frac{M_{cb}}{M_e}\right)^3 + \left(\frac{M_a}{M_e}\right)^2 \exp\left\{\nu\left(\frac{M_a}{M_e} + \frac{M_{cb}}{M_e}\right)\right\}\right] \quad (2)$$

where the parameter $\nu = 1.1 \pm 0.2$; C_1 and C_2 are constant coefficients. Though the form of eqs 1 and 2 are easily rationalized using a drag coupling analysis proposed for star/linear polymer blends by Lee and Archer,[16] the observed frequency dependences of storage and loss moduli for multiarm materials cannot be predicted using this approach. In a forthcoming article we will compare predictions of the stress relaxation dynamics of A_3−**A**−A_3 polymers provided by the H-polymer theory of McLeish and co-workers[2] with our experimental observations.

Conclusions

Relaxation dynamics of several model A_3−**A**−A_3 multiarm 1,4-polybutadiene polymer melts and solutions were investigated using small amplitude oscillatory shear rheometry over a broad temperature range (−90 to +26 °C) and a wide range of solution concentrations. The high frequency, segmental dynamics are found to be essentially insensitive to arm and crossbar molecular weight and to modest differences in arm and crossbar microstructure. Two rubbery plateaus have been identified from loss $G''(\omega)$ minima observed at low frequencies. The first plateau regime is observed at high frequency (prior to the onset of arm relaxation) and is assigned to the entanglement network created by long multiarm polymers, while the second plateau is found at low frequency (after completion of arm relaxation) and has been assigned to the network formed by unrelaxed crossbar A segments, following arm relaxation. These assignments are confirmed by several observations. First, for multiarm polymer melts, the storage modulus $G'(\omega) \approx G_{N0}$ in this first plateau regime is slightly larger than the plateau modulus of entangled linear 1,4-polybutadiene. This is expected because of the larger vinyl content of the crossbars. Second, G_N varies with multiarm polymer concentration ϕ_{pom} as $G_N(\phi_{pom}) = G_{N0}\phi_{pom}{}^{1+\alpha}$, where $\alpha = 1.2 \pm 0.1$, (i.e., in the same way as the plateau modulus of a linear polymer changes with dilution). Finally, the low-frequency plateau modulus

$G_{N,II} \approx G_N(\phi_{pom})\phi_{cb}^{1+\beta}$, with $\beta \approx 1.3$, is nearly exactly what would be expected for dynamics of crossbar segments in a network dilated by relaxed arm segments. Here $\phi_{cb} = M_{cb}/M_{cb} + 6M_a$ is the crossbar volume fraction.

Despite such evidence in support of the idea that relaxed arms dilute the entanglement structure in which crossbar segments relax stress, in much the same way as a low molecular weight solvent, we find that arms exert a profound influence on crossbar dynamics well after they have relaxed. Specifically, in multarm solutions where $M_a/M_e \leq 2M_a/M_{e0}\phi_{pom}^{\alpha}$, the zero-shear viscosity of multiarm polymer solutions vary with ϕ_{pom} in a slightly weaker manner than expected for linear polymers without contour length fluctuations $\eta_0 \sim \phi_{pom}^{2.9\pm9.2}$. On the other hand, in multiarm solutions with $M_a/M_e > 2M_a/M_{e0}\phi_{pom}^{\alpha}$, a transition to much stronger dependence of terminal properties on concentration is observed. Specifically, for arm entanglement densities above 2, zero-shear viscosity and terminal time manifest exponential dependencies on multiarm solution concentration.

Acknowledgment. The authors are grateful to the National Science Foundation (Grant No. DMR9816105) for supporting this study. H NMR measurements were performed using facilities provided by the Cornell Center of Materials Research.

References and Notes

(1) McLeish, T. C. B. *Macromolecules* **1988**, *21*, 1062.
(2) McLeish, T. C. B.; Allgaier, J.; Bick, D. K.; Bishko, G.; Biswas, P.; Blackwell, R.; Blotteiere, B.; Clarke, N.; Gibbs, B.; Groves, D. J.; Hakiki, A.; Heenan, R. K.; Johnson, J. M.; Kant, R.; Read, D. J.; Young, R. N. *Macromolecules* **1999**, *32*, 6734.
(3) Daniels, D. R.; McLeish, T. C. B.; Crosby, B. J.; Young, R. N.; Fernyhough, C. M. *Macromolecules* **2001**, *34*, 7025.
(4) Larson, R. G *Macromolecules* **2001**, *34*, 4556.
(5) Roovers, J. *Macromolecules* **1984**, *17*, 1196.
(6) Roovers, J.; Toporowski, P. M. *Macromolecules* **1987**, *20*, 2300.
(7) Daniels, D. R.; McLeish, T. C. B.; Kant, R.; Crosby, B. J.; Young, R. N.; Pryke, A.; Allgaier, J.; Groves, D. J.; Hawkins R. J. *Rheol. Acta* **2001**, *40*, 403.
(8) Archer, L. A.; Varshney, S. K. *Macromolecules* **1998**, *31*, 6348.
(9) Islam, M. T.; Juliani, J.; Archer, L. A.; Varshney, S. K. *Macromolecules* **2001**, *34*, 6438.
(10) Salle, R.; Pham, Q. T. *J. Polym. Sci.* **1977**, *15*, 1799.
(11) Juliani; Archer, L. A. *J. Rheol.* **2001**, *45*, 691.
(12) Ferry, J. D. *Viscoelastic Properties of Polymers*, 3rd ed.; Wiley: New York, 1980.
(13) Dao, T. T.; Archer, L. A. *Langmuir* **2001**, *17*, 4042.
(14) Colby, R. H.; Rubinstein, M. *Macromolecules* **1990**, *23*, 2753.
(15) Lusignan, C. P.; Mourey, T. H.; Wilson, J. C.; Colby, R. H. *Phys. Rev. E* **1999**, *60*, 5657.
(16) Lee, J. H.; Archer, L. A. *J. Polym. Sci., Part B: Polym. Phys.* **2001**, *39*, 2501.

MA0205010